JOURNAL OF APPLIED BIOMECHANICS, 1994, **10**, 95-109

A Mathematical Model for the Trajectory of a Spiked Volleyball and Its Coaching Application

Shawn S. Kao, Richard W. Sellens, and Joan M. Stevenson

A wind tunnel test was conducted to empirically determine the relationship between the Magnus force (M), spin rate (ω), and linear velocity (V) of a spiked volleyball. This relationship was applied in a two-dimensional mathematical model for the trajectory of the spiked volleyball. After being validated mathematically and empirically, the model was used to analyze three facets of play that a coach must address: the importance of topspin, possibility of overblock spiking, and optimum spiking points. It was found that topspin can increase the spiking effectiveness dramatically in many ways. It was also found that a shot spiked from about 2 m behind the net has the least possibility of being blocked.

Part 1: Development of the Model

The spike is the most commonly used and the most powerful offensive weapon in the game of volleyball, so any new knowledge that helps athletes improve spiking effectiveness will develop the game. Biomechanists have been trying to improve athletes' performances since biomechanics evolved in the 1970s, and the results have been very successful (Samson & Roy, 1975). However, few papers in the literature have dealt with the trajectory of the spiked volleyball (Coleman, Benham, & Northcott, 1993; Li, 1983).

Many papers on the trajectory of a spinning sphere are available in the literature (Bearman & Harvey, 1976; Briggs, 1959; Watts & Ferrer, 1987). However, experimental studies of spinning spheres have been limited to the measurement of Magnus and drag forces on the shape of the ball's trajectory in games such as tennis, baseball, and golf (Erlichson, 1983; Mcphee & Andrews, 1988; Zufiria & Sanmartin, 1982).

The fact that tennis balls curve because of the spin imparted to them has been well documented for a long time (Rayleigh, 1869). This phenomenon, the

Shawn S. Kao and Joan M. Stevenson are with the School of Physical and Health Education, and Richard W. Sellens is with the Department of Mechanical Engineering, Queen's University, Kingston, ON, Canada K7L 3N6.

Magnus effect, was named for a German engineer, G. Magnus, who first described the lateral deflection of a spinning cylinder and sphere. The *Magnus force*, defined as the force that causes the deflection of spinning objects, is often referred to as *lift* in the literature. However, it acts in a direction perpendicular to the axis of spin, which may yield a force in a direction other than vertical. Therefore, the two terms are not interchangeable.

The first and most systematic experimental determination of the forces acting on a spinning baseball was conducted by Briggs (1959). A spinning baseball with known rate of rotation was dropped across a horizontal wind tunnel in which the velocity of the air was known, and the deflection of the ball's path due to spin was measured. Using the measured lateral deflections, Briggs calculated the necessary lateral forces. Briggs reported that the lateral force was proportional to the product of the square of the wind tunnel speed (V^2) and the rotation rate of the ball (ω).

However, classical inviscid flow theory (White, 1986) for a two-dimensional body with circulation predicts a force on the body proportional to flow velocity (V) and circulation or spin (ω). By analogy, one would expect that the Magnus force on a spinning sphere would also be proportional to ωV rather than to ωV^2, as found by Briggs (1959). Experiments by Bearman and Harvey (1976) on golf balls and Watts and Ferrer (1987) on baseballs have found the Magnus force to be proportional to ωV.

While these results appear contradictory, it is important to note that most ball games involve Reynolds numbers (Re) that lie in the vicinity of the so-called drag crisis (White, 1986). The drag coefficient for spheres drops sharply at around $Re = 4 \cdot 10^5$ due to transition between laminar and turbulent flow. For example, a volleyball travelling at 30 $m \cdot s^{-1}$ in air at 1 atmosphere and 20 °C has a Reynolds number of $4 \cdot 10^5$. Since flow effects are generally proportional to V in laminar flow and V^2 in turbulent flow, one might expect the results to be strongly dependent on the particular flow conditions including such factors as Reynolds numbers and the surface characteristics of the sphere.

Thus, it is important to perform tests for the particular geometry and flow conditions associated with a spiked volleyball. As detailed later in this paper, such measurements provided a correlation for the Magnus force on the spinning ball, which is used in the these predictions. Various mathematical approaches are available to calculate the trajectory once the various forces are known (Frohlich, 1983; Rex, 1985; Štěpánek, 1988).

Two-Dimensional Trajectory Equations

A 2-D model for the trajectory may be developed based on the coordinate system shown in Figure 1a, if we assume that the axis of rotation of the ball is horizontal. This is a reasonable assumption, since purely horizontal rotation represents an optimum spike. The ball is subject to Magnus (M), drag (D), and gravitational forces (mg) as shown in Figure 1b. The directions of both the Magnus and drag forces depend on the direction of travel of the ball. Their magnitudes may be expressed as

$$M = C_M \omega^a V^b \tag{1}$$

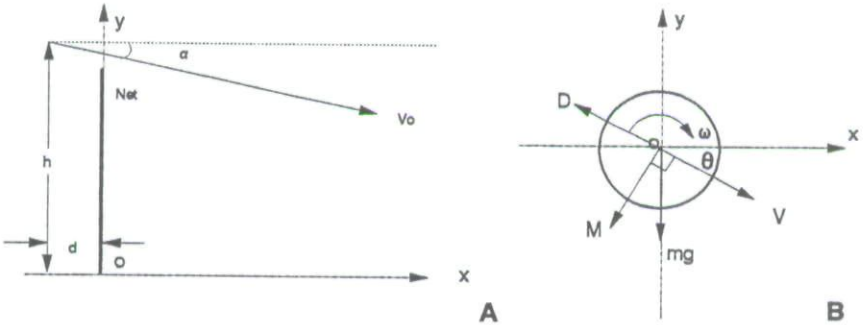

Figure 1 — (a) Volleyball court in a two-dimensional Cartesian coordinate system with the initial conditions of a spiked volleyball. (b) The three forces to which a spiked volleyball reacts.

$$D = \frac{1}{2}C_D\rho AV^2 \tag{2}$$

where C_M, a, and b are constants determined empirically as described later in the paper. C_D is the drag coefficient equal to 0.5 based on Re around $4 \cdot 10^5$, and ρ is the density of the air (White, 1986).

The horizontal and vertical components of the total force on the ball are

$$F_x = -C_M\omega^a V^b \sin\theta - \frac{1}{2}C_D\rho AV^2\cos\theta \tag{3}$$

$$F_Y = -mg - C_M\omega^a V^b\cos\theta + \frac{1}{2}C_D\rho AV^2\sin\theta. \tag{4}$$

Noting that the velocity components are (Figure 1b)

$$\dot{X} = V\cos\theta \tag{5}$$

$$\dot{Y} = -V\sin\theta \tag{6}$$

so that

$$V^2 = \dot{X}^2 + \dot{Y}^2 \tag{7}$$

and applying Newton's second law ($\Sigma F = ma$), one obtains two equations for the acceleration components of the ball with respect to time:

$$\ddot{X} = \frac{C_M\omega^a\dot{Y}(\sqrt{\dot{X}^2 + \dot{Y}^2})^{b-1}}{m} - \frac{\frac{1}{2}C_D\rho A\dot{X}\sqrt{\dot{X}^2 + \dot{Y}^2}}{m} \tag{8}$$

$$\ddot{Y} = -g - \frac{C_M\omega^a\dot{X}(\sqrt{\dot{X}^2 + \dot{Y}^2})^{b-1}}{m} - \frac{\frac{1}{2}C_D\rho A\dot{Y}\sqrt{\dot{X}^2 + \dot{Y}^2}}{m}. \tag{9}$$

These nonlinear ordinary differential equations are readily solved numerically to obtain X and Y, the position of the ball, using a Runge-Kutta scheme, given initial conditions for position and velocity.

Three-Dimensional Trajectory Equations

The volleyball court is considered in a 3-D coordinate system in the following way: The left side line is the X axis, the central line is the Y axis, and the left antenna and its extension are the Z axis, as shown in Figure 2a, with the origin at the intersection of the left side and the central lines.

Since the spin axis of a spiked volleyball is horizontal, its trajectory will lie within a vertical plane because all three forces acting on that ball are in the same plane (see Figure 1b). We will let the Y axis of the 2-D frame be coincident to the Z axis of the 3-D frame; rotate the plane, in which the trajectory exists, counterclockwise about the Z axis by an angle (β); then translate the plane to the position with a spiking point at A (X_0, Y_0) (Figure 2b). Thus, the 3-D equations may be obtained as

$$X_{3D} = -X_{2D}\sin\beta \tag{10}$$

$$Y_{3D} = X_{2D}\cos\beta \tag{11}$$

$$Z_{3D} = Y_{2D}. \tag{12}$$

These are not fully three-dimensional equations, because the ball never leaves the plane in which it moves initially, since the spin axis of the volleyball was fixed to horizontal in order to create pure topspin. In future work the model should be expanded to include the general case of orientations of rotation axes in order to accommodate problems such as sidespin.

Experimental Methods and Results

The derived mathematical model cannot be applied to situations in volleyball until the unknowns in the model have been determined and the model properly validated. The following experiments were aimed at these purposes.

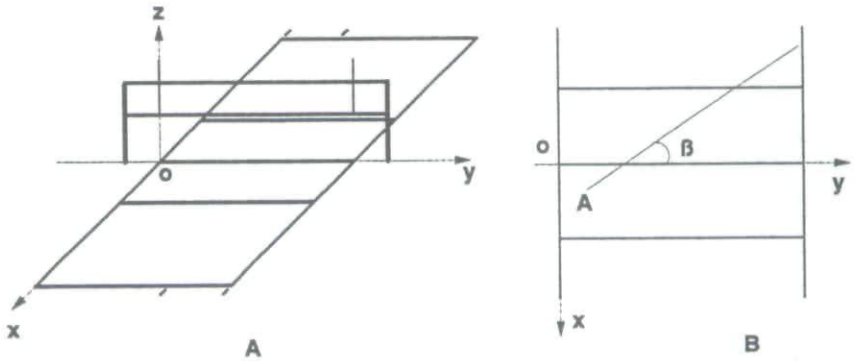

Figure 2 — (a) Volleyball court in a three-dimensional Cartesian coordinate system. (b) Top view of a volleyball court with the projection of a trajectory of a spiked volleyball.

Linear and Angular Velocities of a Spiked Volleyball. To assure that the wind tunnel testing was carried out under appropriate conditions, both the linear and angular velocities of a spiked volleyball had to be determined. It has been reported that top volleyball hitters can spike a ball at a linear velocity of 30 m · s^{-1} (Frohlich, 1983). However, no researchers have reported the amount of the angular velocity on a spiked volleyball. Therefore, an experiment was conducted to identify the typical range of the linear and angular velocities of volleyballs as spiked by highly skilled volleyball players.

Ten male players from the 1991 Ontario Provincial Team volunteered to execute 30 spikes under experimental conditions. The filming site involved two synchronized video cameras with high-speed shutters (1/500 s). The cameras were oriented at right angles to each other and were synchronized electronically. The players were asked to spike the ball with maximum velocity along a target line, which was perpendicular to the axis of Camera 1, on the floor. Camera 2 was aligned with the target line, facing the oncoming balls. Three specially marked volleyballs were used, so that rotation of the ball could be tracked and recorded. The sampling rate was 30 frames · s^{-1}.

We digitized the trials from Camera 1 using the Peak Performance Analyzing System and estimated linear velocities from the first three fields after ball contact. The rotation rate of the spiked volleyball was counted from multiple fields on the tape from Camera 2. Because only an approximate range of the linear and angular velocity was needed to set up the wind tunnel conditions, we did not smooth the data or analyze error. For these subjects, the average linear velocity was calculated to be 19.85 ± 1.89 m · s^{-1} while the angular velocity was 5.79 ± 1.08 rev · s^{-1}. Based on this experiment and the linear velocities reported by other researchers (Coleman et al., 1993; Li, 1983; Maxwell, 1980), representative ranges of the linear and angular velocities of a hard-spiked volleyball from highly skilled players were considered to be 15–35 m · s^{-1} and 3–8 rev · s^{-1}, respectively.

Measurement of the Magnus Force on a Volleyball. A device for mounting a spinning volleyball in a wind tunnel is shown in Figure 3. The basic principle used in the device was that of a simple balance. An official Olympic volleyball, inflated to the standard criteria, was glued on a specially made aluminum dish that was screwed to the end of a 1/2-in.-diameter steel shaft. The shaft was driven by a small motor mounted on a plate. The plate was connected to the side wall of the wind tunnel by a hinge whose axis of rotation was horizontal so that the plate with the motor on it could move freely up and down. The shaft was fixed on the plate by two self-adjusting bearings and extended through a hole in the wall into the wind tunnel where the ball was mounted. The length of the shaft was adjusted in order to place the ball in the center of the wind tunnel. Because the motor side of the system was significantly heavier than the ball side, a pulley system was used to counterbalance it. Weights were applied to the pulley system to balance the whole system.

As a force (M) was applied to the ball, it created a counterclockwise moment about the fulcrum, and the whole system was moved out of balance. To rebalance the system, a force (W) was applied on the motor side to create a clockwise moment that was equal to the moment created by M. For simplicity, weights were placed at point P (see Figure 3), at an equal distance from the fulcrum as was the center of the ball. In this way, we directly monitored force

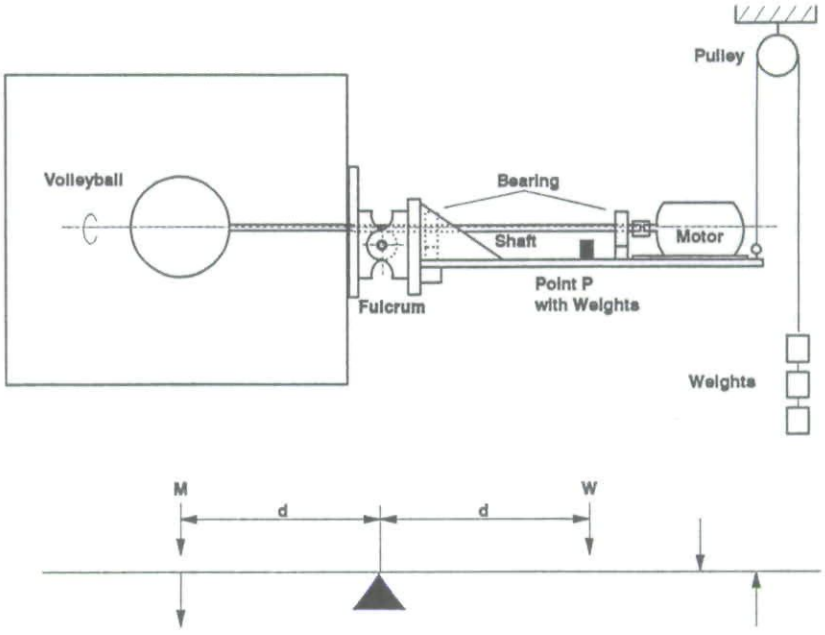

Figure 3 — The balance for wind tunnel testing of the Magnus force experienced by a volleyball. In this side view, the air flow is directly toward the viewer.

changes on the ball (M) at point P on the motor side by loading and unloading weights (W) to keep the whole system in balance.

The motor used in the test was a DC variable-speed, reversible motor. A motor controller was used to control the rate and the rotating direction of the motor. Tests were performed in a low-speed wind tunnel with the inner dimensions 0.7 m in width and 0.6 m in height. The flow speed in the wind tunnel could be varied and was monitored by a hot wire anemometer. The rate of rotation of the motor, and thus the ball, was measured with a strobe-light tachometer suspended directly above the shaft so that the rate of rotation could be monitored without interfering with the rotation or the balance. The pulley, with a ball-bearing axle, was fixed above the end of the plate and aligned to minimize the mechanical friction. All the turning points were lubricated.

The motor was set to an angular velocity 3–8 rev $\cdot$ s^{-1} in the direction of rotation to create a downward Magnus force on the ball. Weights were put at point P and the balance was broken. The wind tunnel fan was then started so that the air in the tunnel produced a downward Magnus force on the ball. The air speed was altered to increase the Magnus force on the ball so as to return the whole system to balance again. Then anemometer and tachometer readings and the weight were recorded. The weight was increased systematically and the balancing process repeated to obtain further data points. Repeating the process yielded a full matrix of data for five different nominal rates of rotation.

As described previously, we concluded that the Magnus force (M) on a spinning ball was shown as Equation 1. Using the measured data, we selected values of C_M, a, and b to minimize the mean square error between those data and the correlation in Equation 1. Figure 4 shows the results of the wind tunnel

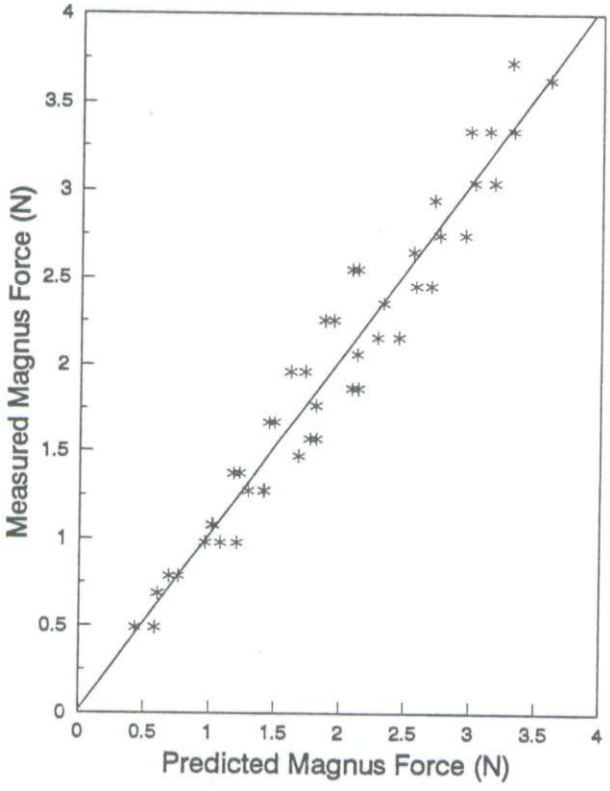

Figure 4 — Results of the wind tunnel tests.

tests, in which the measured Magnus force is plotted against the Magnus force predicted by the correlation equation of the best fit,

$$M = 0.000041\ \omega^{0.8}\ V^{2.4}. \tag{13}$$

The squared correlation coefficient (R^2) for the regression was 0.946.

Validation of the Model. The model was validated in two ways: mathematically and empirically. First of all, we solved Equations 8 and 9 to get the trajectory coordinates by the second-order accurate Runge-Kutta methods, using Equation 13 to evaluate the Magnus force and Equation 2 to evaluate the drag force.

If there was no spin on the ball and no drag, the trajectory would be a parabola. Figure 5 shows a comparison of the calculated trajectory from the model without spin and drag ($C_D = 0$, $\omega = 0$ rev $\cdot$ s^{-1}) with a parabola calculated from the analytical solution using the same initial conditions. There was a slight deviation between the two, due to step size (0.01) in the numerical method. Figure 5 also shows a comparison of the trajectories with ($C_D = 0.5$) and without ($C_D = 0$) drag. The trajectory with drag was slowed down and landed closer to the spiking point than the one without drag. These results were expected and confirmed the physical and mathematical correctness of the model.

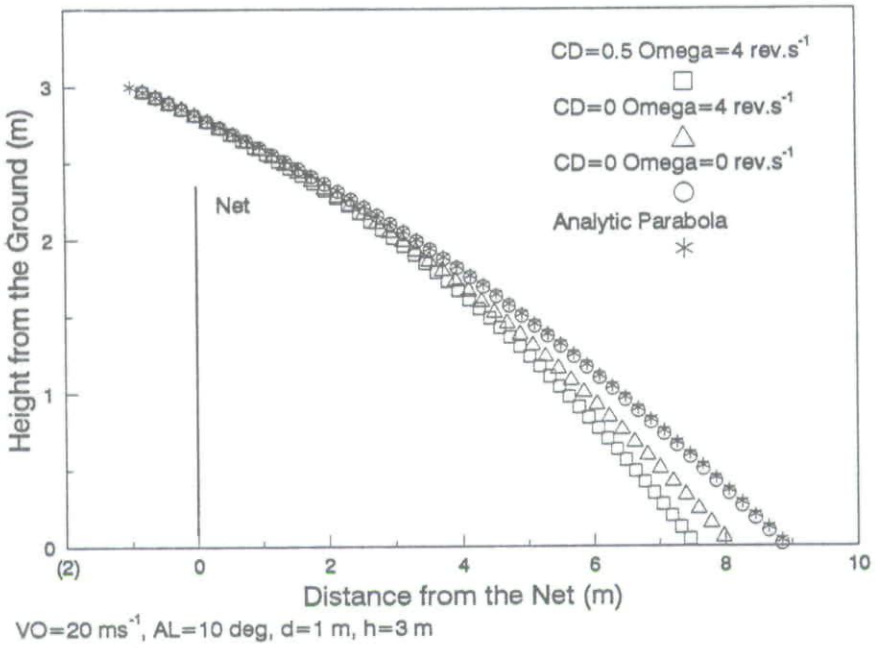

Figure 5 — Mathematical validation of the model.

In empirical validation, the calculated trajectory was compared with the real trajectory of a spiked volleyball. A filming site was set up in a gymnasium, as shown by the inset in Figure 6. A well-skilled spiker stood at the hitting point and completed 30 spikes. Only 10 out of the 30 trials were considered for analysis because either the rotation of the ball was not pure topspin or the ball was hit out of the filming plane. The videotape from Camera 1 was digitized to obtain V_0, α, d, and h (refer to Figure 1a for α, d, and h) with ω obtained from Camera 2. These data were used as the initial conditions for the model. We determined the actual volleyball trajectories by digitizing the location of the ball in each frame of a trial from Camera 1. Figure 6 is one example of the comparison of the calculated trajectory with the digitized one. Based on an error analysis to minimize the difference between the model and actual trajectory profiles, the drag coefficient was changed from 0.5 to 0.2 for better match.

Discussion and Conclusion

1. The functional equation of the Magnus force experienced by a spiked volleyball (Equation 13) found in this study more closely matches what Briggs (1959) reported than what Watts and Ferrer (1987) found, despite the fact that both studies analyzed baseballs. When this equation was used to evaluate the Magnus force in the validation, there was no substantial difference between the calculated and the digitized trajectories (see Figure 6). This correlation ($R^2 = 0.946$) stays consistent at least in the range ω: 3–8 rev $\cdot$ s^{-1}, V: 15–35 m $\cdot$ s^{-1} for a volleyball. If the baseball data of Watts and Ferrer (1987) (where a = 1, b = 1) and Briggs

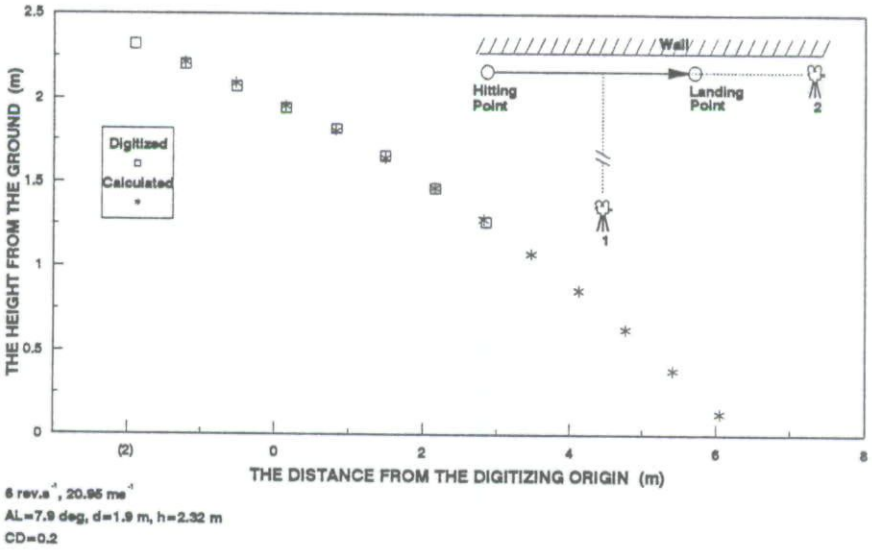

Figure 6 — Empirical validation of the model.

(1959) (where a = 1, b = 2) were used, the plotted results would have been more scattered with R^2s of only 0.647 and 0.874, respectively.

2. The Reynolds number of the spiked volleyball theoretically places the drag coefficient C_D very close to the "drag crisis." As V_0 changes, C_D may vary dramatically, but this does not change the trajectory substantially. Had C_D varied between 0.1 to 0.5, the largest range of theoretical change based on the Reynolds number, the trajectory would have changed even less than what is shown in Figure 5, with C_D changing from 0 to 0.5. From the validation, it was determined that 0.2 was a better estimate of value for C_D when V_0 was around 20 $m \cdot s^{-1}$. To verify this coefficient, further wind tunnel experimentation would be required.

3. It was concluded that the differential equations for the trajectory of a spiked volleyball (Equations 8 and 9), the Magnus force equation (Equation 13), and the drag force equation (Equation 2) with $C_D = 0.2$ are valid and can be used in a mathematical model of the volleyball spike trajectory.

Part 2: Applications of the Model

Since the service reception (the prerequisite for a tactical combination attack in volleyball) is not always perfect, many of the attacks have to be initiated with a high set to power spikers at the sides of the net, which means that the opponents have enough time to form a solid double block. High sets to power spikers happen even more frequently in counterattacks because the digs usually are not good enough to run complex tactics. Thus, studying power attacks from sides of the net is still practical in modern volleyball (Samson & Roy, 1975).

The purpose of these applications was to use the model to answer coaching questions involving power attack strategies where double blocks would be in

position. To accomplish these objectives, computer programs were developed to investigate the relationship between the flight path of a spiked volleyball, block locations, and ball landing locations. By changing the input conditions to simulate the different game situations, we have used the model to study the impact of those changes.

The Importance of Topspin

The faster the topspin on the spiked volleyball, the closer the ball lands to the hitting point. Volleyball coaches have been aware of this effect for decades but have no assessment strategy available to them. The purpose of this application was to examine the importance of topspin on landing location in order to gain insight into its importance as a coaching point.

The spiking conditions are illustrated Figure 1a with the spike trajectory illustrated in Figure 2b. To study the effect of topspin, we used six spin rates from 0 to 10 rev $\cdot$ s^{-1}. The other input conditions were fixed at $V_0 = 20$ m $\cdot$ s^{-1}, $\alpha = 5°$, d = 1 m, and h = 3 m. An analysis of the landing distances corresponding to each trial was given as output from a computer program.

Figure 7 shows the six trajectories corresponding to each rate of the topspin. With all the other initial conditions fixed, a spin rate of 10 rev $\cdot$ s^{-1} brings the ball 1.83 m closer to the net than the landing point of the nonspinning ball. Another way to make the ball land 1.83 m closer, without using topspin, is to increase the spiking angle of depression α from 5° to 9°. This strategy, however, will decrease the height of the ball when it is crossing the net from 2.90 to 2.82 m. This will significantly increase the possibility of the shot being blocked. The equivalent height loss at the net with 10 rev $\cdot$ s^{-1} of topspin is only 2.90 to 2.89 m, a negligible amount. Without sacrificing linear velocity, volleyball spikers

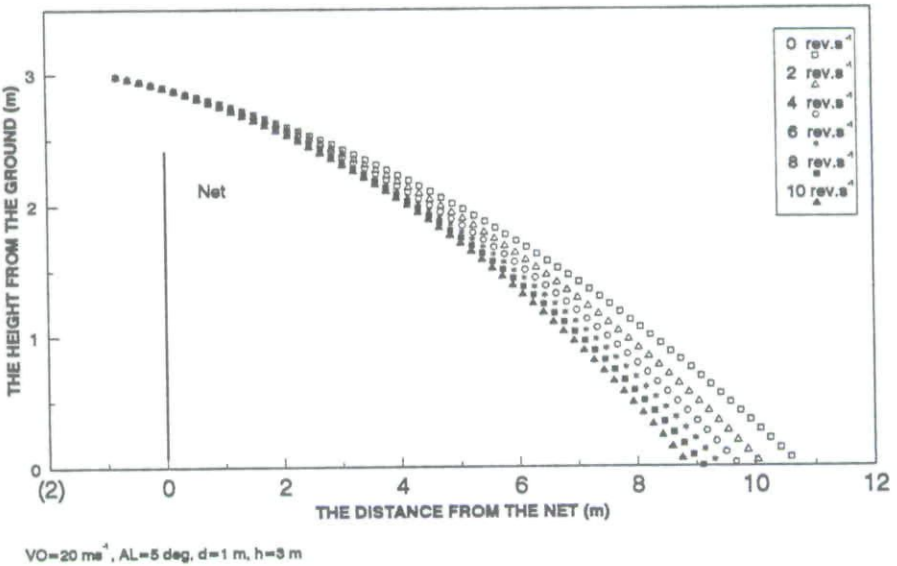

Figure 7 — The importance of topspin in volleyball spikes.

should try to put as much topspin on the ball as possible, because even a few rotations per second of topspin will change the trajectory shape of a spiked volleyball dramatically in such a way that the ball lands closer and earlier without decreasing the ball height at the net.

Possibility of Overblock Spiking

A crosscourt spike to the opposite corner of the court creates the greatest displacement and, therefore, the best opportunity of spiking over a block. The model was used to obtain a crosscourt trajectory that landed precisely at the opposite corner, thus giving the maximum possible ball height at the net, or the maximum block height that could be successfully beaten by this spike. In order to help coaches assess the spiking characteristics needed for a power spiker to spike over a block, we developed a computer program to investigate the relationship of the maximum height at the net and the initial linear and angular velocities.

For this example, the spiking point was fixed at 3.2 m above the floor, 1.5 m behind the net, and 1.0 m inside the left sideline. The linear velocity was varied from 15 to 30 m · s^{-1} and the angular velocity was varied from 4 to 12 rev · s^{-1}.

Figure 8 is a contour graph showing the result of the computer analysis. It shows the maximum height at the net as a function of the initial linear velocity V_0 and angular velocity ω. For instance, with a linear velocity of 25 m · s^{-1} and an angular velocity of 4 rev · s^{-1}, a spiker can beat a block of 3.05 m at that spiking point. To clear a block of 3.10 m for the same linear velocity, the spiker must impart at least 7.5 rev · s^{-1} topspin to the ball. A ball hit with a low linear

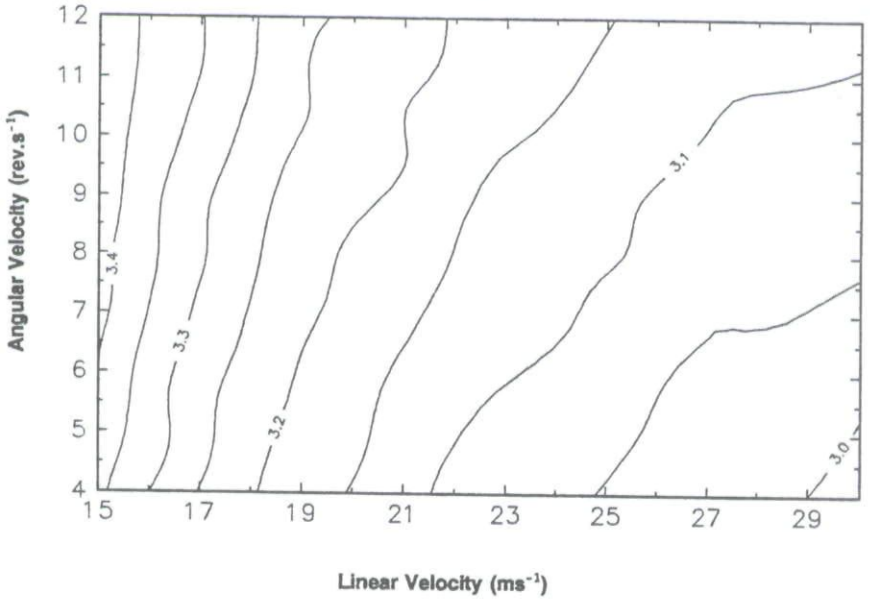

Figure 8 — Trajectory height over net as a function of angular and linear velocity.

velocity of 15 m · s^{-1} and an angular velocity of 6.5 rev · s^{-1} can clear a 3.40-m block at the same spiking point. However, it takes the ball a longer time to land, thus giving the defenders adequate time to move and dig the ball. The slope of the contours becomes flatter as the initial linear velocity increases. This means that the faster a ball is hit, the greater is the importance of topspin in making the ball clear the block and land inbounds.

The Optimum Spiking Points

In this paper, the optimum spiking point is defined as the point from which the ball is spiked with the largest open angle, assuming the block is also in the optimum location for maximum court protection. A spiker can spike either a straight line AF or a crosscourt line AB from one point in the court (Figure 9). The intercept of these lines creates an angle BAF through which the spiker can successfully spike the ball. If AB and AF are such trajectories that just clear the net and then land right on the sideline, then angle BAF is the largest one within which the spiker can hit the ball through from A. However, a part of angle BAF (angle CAE) is blocked by two blockers. In this study, the block is assumed to be in the center because it is a more common strategy to gain the maximum court coverage. The other parts of the angle that have not been blocked are the only paths to clear around the block. Given spiking characteristics, there is a point where the sum of the two unblocked angles BAC and EAF is the largest, thus minimizing the possibility of being blocked. The purpose of this application is to determine this optimum point, in front of the attack line, for a power spiker to hit around a block.

With the aid of a computer program, point A was moved from the left sideline to the court center in 0.25-m increments and from 0.5 m behind the center line to 0.5 m in front of the attack line in 0.25-m increments to represent the various positions from which a spiker would hit the ball. Because the volleyball

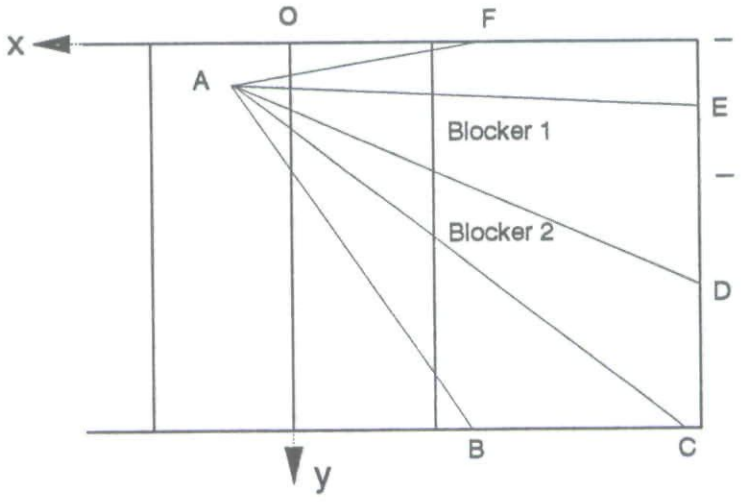

Figure 9 — Schematic diagram of the optimum spiking point.

court is symmetrical, the analysis results for the left half-court can be reversed (mirror reflection) onto the right half to cover the whole attacking zone. For each location, angles BAC and EAF were calculated to yield the largest sum of the two angles, thus the optimum spiking location.

Figure 10 is a contour graph showing the open angles (BAC + EAF) in degrees available to the power spiker who spikes the ball with an initial linear velocity of 20 m · s^{-1} and an angular velocity of 7 rev · s^{-1} at a hitting height of 3 m. The block width was 1.20 m. According to the graph, the optimum spiking points that provide a 30° open spiking angle vary from 1.6–2.5 m behind the net to 0–1.5 m inside the sideline. It is interesting to note that the sets for a back-row attack in modern volleyball are usually in this area, which happens to have the largest open angle. This is probably one of the reasons that back-row attacking has a high success rate: because it always executed from the area that has a reduced possibility to be blocked.

Conclusions

A numerical model of volleyball spiking trajectories has been applied successfully to deal with questions of the advantage of topspin, chances of overblock spiking, and optimum location for spiking around a block. The characteristics of this model could also be used to evaluate the trajectories of spike serves that are being used in modern volleyball. All of these questions are of great practical importance to coaches.

1. If all other conditions were held constant, a volleyball served with topspin would land 1.83 m closer to the net than would a ball with no spin.

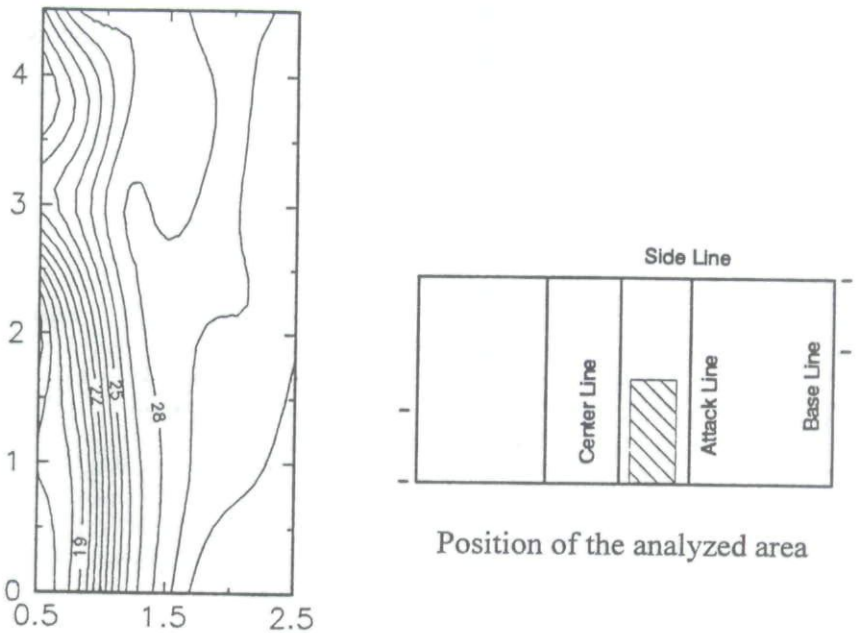

Figure 10 — Open spiking angle as a function of spiking point.

Therefore, athletes should be encouraged to hit with as much topspin as possible, without sacrificing linear velocity.

2. A contour graph was developed to demonstrate what type of linear and angular velocities would be necessary to hit over a double block. Coaches could analyze specific athletes' abilities to determine whether athletes should attempt overblock spiking.

3. A contour graph was developed to determine the optimum spiking points players should use to hit around a double block. Results showed that spikes from the corners and 1.5–2.5 m behind the net give players the best chance of hitting around a double block. In addition, back-row attackers have a strong chance of hitting around the block because they have the largest open court angles.

The practical examples provided by the applications of the model show the insights that can be gained by a scientific approach to trajectory analysis. The greatest advantage of this model is that it can be applied to specific athletes, who will each have different abilities for height, speed, and spin. This individualized approach will be best addressed by developing software, thus allowing coaches direct access to the model, so that they can answer questions specific to their own teams.

References

Bearman, P.W., & Harvey, J. K. (1976). Golf ball aerodynamics. *Aeronautical Quarterly*, **27**, 112-122.

Briggs, L. (1959). Effect of spin and speed on the lateral deflection (curve) of a baseball; and the Magnus effect for smooth sphere. *American Journal of Physics*, **27**, 589-600.

Coleman, S.G.S., Benham, A.S., & Northcott, S.R. (1993). A three dimensional cinematographical analysis of the volleyball spike. *Journal of Sports Sciences*, **11**(4), 295-302.

Erlichson, H. (1983). Maximum projectile range with drag and lift, with particular application to golf. *American Journal of Physics*, **51**(4), 357-363.

Frohlich, C. (1983). Aerodynamic drag crisis and its possible effect on the flight of baseballs. *American Journal of Physics*, **52**(4), 325-334.

Li, Z. (1983). Improving the ability of power attack is one of the most important weapons for Chinese men's volleyball team on the way to world champion. *The Symposium of Research Defending Papers for National Volleyball Coach* [in Chinese], 7-8.

Maxwell, T. (1980). A cinematographic analysis of the volleyball spike of selected top-calibre female athletes. *Volleyball Technical Journal*, **VII**(1), 43-54.

Mcphee, J., & Andrews, G. (1988). Effect of sidespin and wind on projectile trajectory, with particular application to golf. *American Journal of Physics*, **56**(10), 933-939.

Rayleigh, L. (1869). On the irregular flight of a tennis ball. *Scientific Papers*, **1**, 344.

Rex, A. (1985). The effect of spin on the flight of batted baseballs. *American Journal of Physics*, **53**(11), 1073-1075.

Samson, J., & Roy, B. (1975). Biomechanical analysis of the volleyball spike. In P.V. Komi (Ed.), *Biomechanics V-B* (pp. 332-336). Baltimore: University Park Press.

Štěpánek, A. (1988). The aerodynamics of tennis balls—The topspin lob. *American Journal of Physics*, **56**(2), 138-142.

Watts, R., & Ferrer, R. (1987). The lateral force on a spinning sphere: Aerodynamics of a curveball. *American Journal of Physics*, **55**(1), 40-44.

White, F.M. (1986). *Fluid mechanics*. New York: McGraw-Hill.

Zufiria, J., & Sanmartin, J. (1982). Influence of air drag on the optimal hand launching of a small, round projectile. *American Journal of Physics*, **50**(1), 59-64.